Parker Solar Probe FIELDS instrument charging in the near Sun environment: Part II – Comparison of In-Flight Data and Modeling Results

M.F. Diaz-Aguado[1], J.W. Bonnell[2], S. D. Bale[3] , J. Wang[4] and M. Gruntman[4]

[1]Millenium Engineering and Integration, NASA Ames Research Center, Moffett Field, California, USA

[2]Space Sciences Lab, University of California Berkeley, Berkeley, California, USA

[3]Department of Physics, University of California Berkeley, Berkeley, California, USA

[4] Astronautical Engineering Department, University of Southern California, Los Angeles, California, USA

Corresponding author: Millan Fernando Diaz-Aguado (millan.f.diaz-aguado@nasa.gov)

Key Points:

- We predict the floating potentials of the Parker Solar Probe FIELDS antennas.
- We analyze the model antenna I-V curves to determine the optimal current and voltage biases for maximum sensor sensitivity.
- We compare the theoretical predictions with mission flight data and find qualitative agreement, but some quantitative differences.

Abstract

This research shows Part II of the Spacecraft Interaction Plasma Software (SPIS) used to model the Parker Solar Probe (PSP) FIELDS instrument and its interactions with the Solar Wind. Flight data was used to run the PSP model and compared with models using past predicted parameters. The effect of voltage biasing between the antenna, its shield, and the spacecraft on the current balance of each surface was investigated at first perihelion (0.16AU). The model data was reduced to I-V curves to find current saturations (analysis results 52μA versus flight results 54-72 μA), and sheath resistances (analysis results of 307 kΩ versus flight results of 51 kΩ). The recommended bias current to ensure optimal sensitivity of the FIELDS antenna was between -52 μA and -22 μA, which corresponded to a differential potential with respect to the spacecraft between -5V and 5V. The analysis also shows that plasma sheath of the FIELDS antenna and the plasma sheath of the FIELDS shield interacted between each other with an impedance of ~220kΩ.

Plain Language Summary

Measuring the electric field in a space plasma is important for understanding how plasma flows are driven, charge particles are accelerated and heated, and how electromagnetic waves propagate. Measuring the voltage difference between two spatially separated electrodes immersed in a space plasma is one way to estimate the electric field that is present in the plasma. Interpretation of these voltage differences is complicated by the fact that the electrodes often float at a significant voltage relative to the nearby plasma so as to achieve current balance between the electrode and the charged particle environment around it. Different surfaces will float to different potentials depending upon their surface materials, their location relative to other surfaces, their orientation relative to the Sun's light and solar wind flows, and numerical modeling is required to accurately predict how all these factors influence what is observed. Comparison between such numerical models and in situ measurements of potentials and currents, allows one to better understand how the instrument works, and how to operate it better to produce the highest quality electric field estimates.

1 Introduction

As explained in Part I [*Diaz-Aguado et al. '20*], FIELDS is an instrument of the NASA Parker Solar Probe (PSP), a mission to study the Sun. It is composed of five Langmuir Probes and several magnetometers (two three-axis fluxgate magnetometers and one three-axis searchcoil magnetometer). Langmuir Probes are used to measure the density and plasma potential variations of the environment with respect to the probes, as has been done in the laboratory and on many prior missions [*Mott-Smith et al. '26, Garrett '81, Whipple '81, Gurnett et al. '95, Gustafsson et al. '97, Gurnett et al. '04, Vaivads et al. '07, Bonnell et al. '08, Wygant et al. '13, Andersson et al. '15, Bale et al. '16, Torbert et al. '16*]. Predicting the spacecraft charging environment is important for accurate interpretation of probe measurements. [*Feuerbacher et al. '72, Grard '73, Whipple '81, Mullen et al. '86*]. Knowledge of the surface properties of the spacecraft is crucial for estimating the charging behavior of the probes. These surface properties include the photoemission yield, secondary electron emission yield, and backscattered electrons yield.

The FIELDS instrument measures the magnetic fluctuations and electric fields, plasma wave spectra and polarization properties, the spacecraft floating potential and solar radio emissions[*Bale et al. '16*]. PSP is currently operating at distances between 1AU and 0.16 AU (35Rs) away from the Sun. This research paper focuses on the third perihelion. PSP will eventually reach 0.046AU (9.8Rs) away from the Sun.

This paper continues the studies of the FIELDS antennas, the FIELDS shields, the PSP spacecraft, and their interaction with each other and the environment and focuses on the bias potential of the probes and flight data comparison. The FIELDS antennas are four 2m long probes (0.0031m diameter), which are coupled to create double probes [*Bale et al. '16*]. The probes are designed with an active control of the probes by forcing a current from the probes to the spacecraft to be able to change the potential of the probes. Double probe measurements of electric fields were first launched on S3-3 spacecraft [*Mozer et al. '79*]. It was followed by other missions, including GEOS-1, GEOS-2, ISEE-1, Viking, Geotail, Van Allen Probes, PSP and many others.

Figure 1 shows the FIELDS antenna and shield with the bottom of the PSP bus, radiators and Thermal Protection System (TPS). The Sun is located in the -Z direction, with the TPS

thermally protecting the rest of the PSP spacecraft. The FIELDS shields protect the stub of the antenna as it connects to the hinge and from there to the rest of the FIELDS instrument which is shielded from the Sun by the TPS. Previous PSP models did not include the entirety of the FIELDS instrument nor geometry and did not have the proper material properties to perform a full spacecraft charging simulation [*Donegan et al. '10, Ergun et al. '10, Guillemant et al. '12, Donegan et al. '14*].

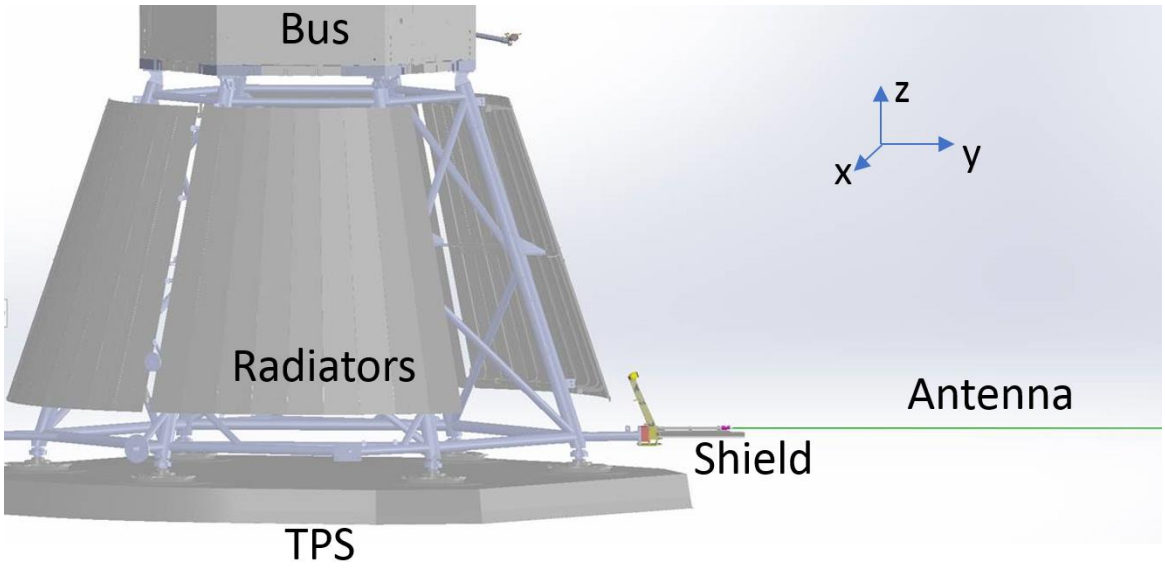

Figure 1 – CAD rendering of PSP with one FIELDS Antenna deployed.

The PSP FIELDS instrument shield, antenna and stub are made with a new material, Nb-C103, with spacecraft charging properties previously unknown. The testing campaign obtained the material processes for photoemission, secondary electron emission, and backscattered SE emission. [*Diaz-Aguado et al. '19, Diaz-Aguado et al. '20*] .

The Spacecraft Plasma Interaction Software (SPIS) [*Roussel et al. '08, Marchand et al. '14*], a self-consistent spacecraft charging software, was used to model PSP and the FIELDS antenna. This open source software can easily include the geometry, and properties of the PSP spacecraft and FIELDS instrument.

The main purpose of this paper is threefold: to continue evaluating the environmental conditions of the PSP FIELDS antennas through modeling the effects of bias potentials; to quantify their effect on measurements of the Solar Wind plasma and to compare them with initial flight data. First the spacecraft charging theory is briefly described, focusing on the bias currents introduced on the antennas. Second, an overview of the SPIS software is provided, followed by

the flight environment and materials used specific to FIELDS and PSP. Finally, the bias potential model results are discussed and compared to flight data.

2 Spacecraft Charging Overview

As has been established through many prior theoretical and observational studies, the potential of a simple conductive object in space is determined by the balance of various charging currents to and from the spacecraft or probe [*Whipple '65, Grard '73, Garrett '81, Whipple '81, Mullen et al. '86, Hastings et al. '96*]. The PSP spacecraft is designed to present a single electrically conductive surface to the environment, except for specific surfaces, including FIELDS antennas and FIELDS shields which remain isolated to be able to make environmental plasma measurements.

The charging of the PSP and FIELDS instrument is solved through balancing the currents on each surface, and can be written as:

$$I(\Phi) = I_{ph}(\Phi) + I_I(\Phi) + I_{se}(\Phi) + I_{bse}(\Phi) + I_e(\Phi) + I_{therm}(\Phi) + I_{other} = 0 \quad (1)$$

where I_{ph} is the photoelectron current from photoelectron emission, I_I and I_e are the ion current and electron current from the plasma environment, respectively, I_{se} secondary electron current, and I_{bse} backscattered secondary electron current resulting from the electrons leaving a surface due to the plasma interaction with surfaces, I_{therrm} thermionic electron current from electrons emitted from a hot body, and I_{other} could be other currents such as sensor bias currents. These currents vary with the spacecraft or probe (Φ) relative to the plasma potential. The currents I_{ph} , I_I , $I_{e,}$, I_{se} , I_{bse} and I_{therm} are studied more in depth in Part I.

From past experience on many magnetospheric and solar wind missions, the application of a negative bias current, I_b to the probe minimizes the offset voltage due to spurious currents to the probe from the spacecraft or environment [*Mozer et al. '79, Pedersen et al. '84, Laakso et al. '95, Pedersen '95, Cully et al. '07*]. A negative bias current is a current of electrons from the spacecraft to the probe. Figure 2 a. shows how for zero bias current (i.e. usual floating potentials) a small change in the ambient current (I_a) translates into a large change in floating potential. Figure 2 b. shows how by adding a bias current, the sensitivity of the probe changes, giving a small voltage differential for the same spurious current variation. The optimal bias current and probe potential can be determined by minimizing the small signal probe impedance R, defined as:

$$R = \left(\frac{dV}{dI}\right)_{V=\Phi} \quad (2)$$

where Φ is the probe potential.

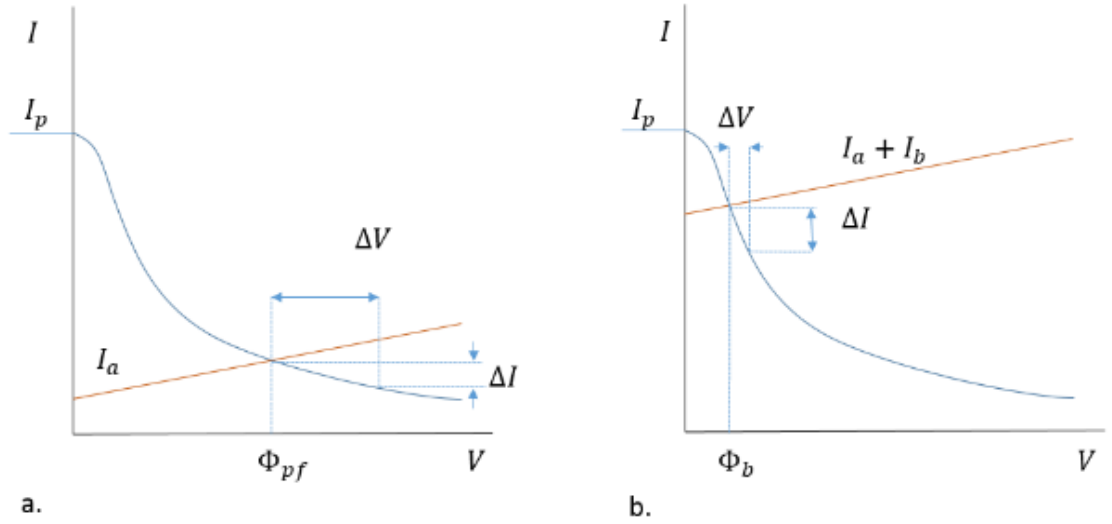

Figure 2 – Bias current schematic where figure a. shows the probe potential and ambient current and b. shows the probe potential and biased current. [*Pedersen '95*]

Sweeping this bias current on FIELDS allows one to determine the I-V curve of the antenna sheath, and thus environmental effects on the antenna and the electric field measurements. Note that SPIS is only able to model a fixed bias voltage between surfaces and then measure the current flowing between those surfaces, as so the I-V curve of the antennas and spacecraft has to be pieced together from multiple runs of the model, as shown in the results section 4.1 below.

3 SPIS Software and Numerical Simulations

The SPIS [*Thiebault '13*] simulation tool was used to model the spacecraft charging characteristics of PSP and FIELDS. It was developed through the European Space Agency (ESA). SPIS is a 3D Particle In Cell (PIC) plasma modeling software. It uses a Vlasov-Poisson equation to consistently solve for the particle density and electric potential distribution. The PSP charging models shown below were implemented using the SPIS package As noted in Part I, new materials and material properties were added to the SPIS database, a careful selection of simulation time step and grid size were chosen, and a suitable meso-thermal model for the SW electrons and ions (protons) was developed. The response of the ambient electrons, photoelectrons (PE), and secondary electrons (SE) to the potential structures around the spacecraft and antennas was modeled using PIC. For more details about SPIS and the PSP model please see Part I.

The 3D model was implemented by placing PSP in a 16m diameter sphere. The PSP spacecraft bus was a 1m diameter cylinder, 1 meter tall. The radiators were modeled as a truncated cone with a 1m diameter on the top, 2m bottom diameter, and 1 meter tall. The TPS was also modeled as a truncated cone with a thickness of 0.12m, 2.48 m bottom diameter, 2.44 top diameter. The FIELDS shield was modeled as a trigonal trapezohedron, 0.32m long, and 0.02m wide. The FIELDS antenna was modeled a 1-D wire, 0.0032m in diameter and 2m long.

The plasma volume was an unstructured mesh with a 1m size at the outer boundary, 10cm at the bus, 8cm at the TPS, 1 cm at the shield and 3cm at the antenna. The mesh size remains several times smaller than the Debye length during the cases shown below.

The modeled properties shown in Table 1 were used for 35Rs pass. The antenna and antenna shield both consist of Nb C103. The TPS shield consists of Al_2O_3 (alumina), the TPS of Carbon-Carbon foam. The radiators were coated with black conductive paint (BWCondPaint). The spacecraft was mostly covered in a conductive black Kapton Multi Layered Insulation (MLI) blanket and a few white conductive radiators.

As shown in Figure 3, the charging model consists of 4 different groups of surfaces, or nodes: spacecraft, Radiators and TPS- foam were node 0; TPS-Sun is node 1; FIELDS Shield is node 2; FIELDS antenna is node 3. As shown in Table 1, the spacecraft, Radiators and TPS foam are considered all to be Node 0. Node 1 is the TPS shield and is connected to Node 0

188 through a variable resistor, which is dependent on the electrical properties of alumina, as shown
189 in Table 2. Node 2 is the antenna and Node 3 is the antenna shield.
190
191 Table 1– Material Properties used in Surface Charging Calculations [*Thiebault '13, Donegan et*
192 *al. '14, Diaz-Aguado et al. '20*]

	Spacecraft	*Radiators*	*TPS Foam*	*TPS-Shield*	*FIELDS shield and antenna*	
Node #	0	0	0	1	Antenna 2/ Shield 3	
Material	BlackKapton	BWCondPaint	Carbon Foam	Al_2O_3	NbC103 Unannealed	NbC103 Annealed
Diaelectric Constant				9.6		
Thickness(m)				1e-4		
Bulk Conductivity (Omega $^{-1}$ m $^{-1}$)	Cond	Cond	Cond	1e-6	Cond	Cond
Effective Atomic Number	5	6.1	4.5	10.2	44.1	44.1
Delta-Max	2.1	1.42	0.93	6.4	1.81	1.97
E-Max (keV)	0.15	0.26	0.28	0.45	0.269	0.252
Range 1 (Angstrom)	71.48	1	180	5	0.733	0.867
Exponent 1	0.6	1.7	0.45	0.1	0.584	0.46
Range 2 (Angstrom)	312.1	1.3	312	1	1.0	1.0
Exponent 2	1.77	0.7	1.95	2.5	1.78	1.71
Proton Yield	0.455	0.287	0.455	0.68	0.244**	0.244**
Proton Max (KeV)	140	1000	80	60	230**	230**
Photoemision (A/m2)	5.00E-06	N/A	N/A	7.80E-05	1.18e-4* +/-0.204e-4	5.75e-5* +/-0.09e-4
Surface Resistivity (omega/square)	Cond	Cond	Cond	Cond	Cond	Cond

193
194 *Average solar min/max photocurrent
195 **Properties not available at the time of publication, used Aluminum instead
196 ***Used Table 2 for Al_2O_3 conductive properties as they are thermally dependent, and therefore
197 dependent on distance to the Sun.
198

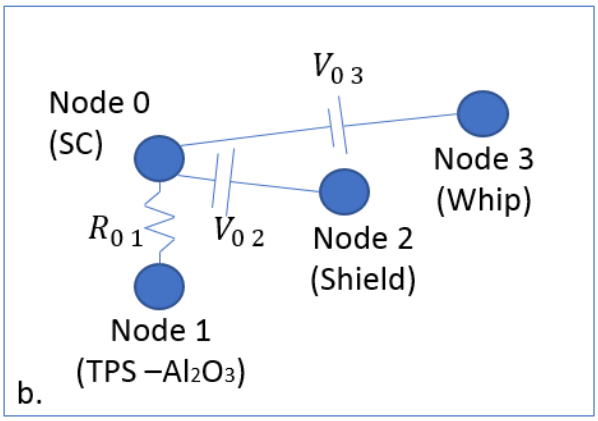

Figure 3 Model circuit design: Voltage biasing of spacecraft and antenna and spacecraft and shield.

The models were run in two configurations: First, Node 2 and Node 3 were free floating to compare with the flight case; second, Node 0 and Node 3 and Node 0 and Node 2 were connected with a variable differential voltage for the first perihelion pass environments only to model the conditions during the inflight I-V bias current sweeps. As noted above, the SPIS circuit module is not able to model a bias current between nodes, so the bias sweep was modeled using a fixed set of bias voltages for which the current flowing between the surfaces was measured, as described below.

Table 2 summarizes the flight data parameters and the previous predicted parameters at 35Rs. The predicted parameters were underestimating the electron density and overestimating the electron and ion temperatures. The SW speed was also higher than predicted.

SPIS uses super-particles injected in each cell to represent dynamics of individual groups of particles. Table 3 shows a selected set of numerical inputs used to model PSP in SPIS at 35Rs. For this analysis, super-particle numbers per cell were 15 for electrons and ions, 5 for photoelectrons, 4 for SE, 3 for BSE and ion induced SE, totaling 22 million super-particles for 35Rs. Steady state during the 35Rs run was reached around 8e-5 sec. The usual computational run-time was 8 hours for 35Rs. The timestep (Dt) was held smaller than usual because the mesh had tetrahedron angles smaller than 60deg. The capacitance of the spacecraft was held at $8\text{x}10^{-10}$ F to speed up the computational time, compared to an estimated $2\text{x}10^{10}$ F. Table 2 also shows the electron plasma frequency, Debye length and electron gyrofrequency.

Table 2 – Predicted plasma parameters[*Bale et al. '16*] at 35Rs compared to flight parameters at 35.7Rs [*Bale et al. '19, Kasper et al. '19, McComas et al. '19*]

		1st Perihelion (Predicted)	*1st Perihelion (Data)*
Plasma Parameter	Units	35 Rs	35.7 Rs
Electron Density	cm^{-3}	281	300-500
Proton Temperature	eV	39.9	8.6-12.9
Electron Temperature	eV	31.8	8.6-12.9*
Magnetic Field Intensity	nT	157	70 to -90
SW Speed	km/s	292	300 to 500
Spacecraft Velocity	km/s	96.8	95.7**
Debye Length	m	2.5	1.29-1.58*
Ion Acoustic Velocity	km/s	78	40.6-49.7*
Electron Gyroradius	m	121	144-166
Electron Plasma Frequency	kHz	150.9	155-201

*Value unknown at this time, assuming ion and electron temperature are similar in value

**Calculated from orbit parameters

In addition to exploring free floating potentials, the authors also explored the current-voltage (I-V) curve for the FIELDS antenna with different shield potentials. An I-V curve study was done at first perihelion with unannealed Nb-C103 material properties varying the bias voltages on the antenna and the shield. Thirty-six cases were studied for antenna and shield voltage offsets relative to spacecraft floating potential from -10V to +10V in increments of 5 V, along with unbiased antenna and shield cases in order to determine the interdependent I-V curves of those surfaces, and to obtain the optimal setting for the antenna bias current.

Table 3 - Typical Numerical Settings for SPIS at 35Rs

	35Rs
Electron Dt	5e-8
Electron Duration	5e-8
Ion Dt	5e-7
Ion Duration	5e-7
SE and Photoem. Dt	5e-8
SE and Photo Duration	5e-8
Plasma Dt	5e-7
Plasma Duration	5e-7
Ion/Electron Super Particle/cell	10-15
Photoemission Super particle/cell	5
SE Super particle/cell	4
SE Ion Super particle/cell	3
Sphere Mesh Size	1 m
Spacecraft Mesh Size	0.1 m
TPS Mesh Size	0.09 m
Shield Mesh Size	0.01 m
Antenna Mesh Size	0.03 m

4 Results

4.1 Numerical Results I-V Curve for FIELDS Antenna and Shield

The following numerical results were completed with the flight estimated Nb-C103 saturation photoelectron current density of 2.4μA/m^2 compared with the laboratory estimate of 1.18 μA/m^2 [Diaz-Aguado et al., 2020]. Figure 4 shows the modeled I-V curves of the antenna at 1st perihelion, or ~35Rs. This curve was obtained by sweeping the bias voltages between the antenna and spacecraft from -10V to 10V, and the shield and spacecraft from -10V to 10V in 5V increments. The curve for the antenna shows similarities to the theoretical I-V curve shown in Part I, Figure 2, for cylindrical probe.

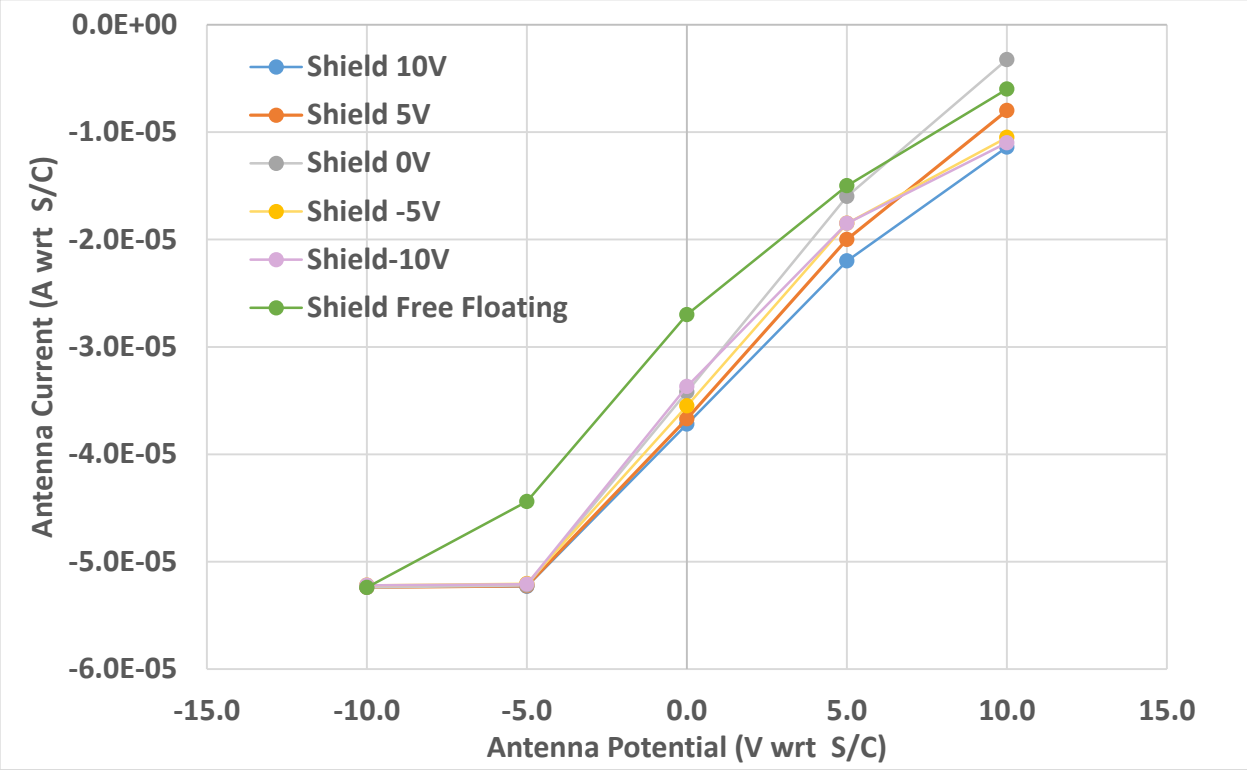

Figure 4– Predicted FIELDS Antenna I-V Curve with Different Shield Bias Potentials.

The recommended bias current to ensure optimal sensitivity of the probe is between -52.1μA and -22.0 μA with respect to the spacecraft, and therefore a voltage differential with respect to the spacecraft between -5V and 5V. The potential of the The slopes of all the I-V curves were similar and did not significantly change depending on the shield potential and correspond to a sheath resistance of ~ 307 kohm. The space potential at the antenna (with respect to infinity) is ~ -5V, described by the first elbow of the I-V curve, and the saturated

current is -53µA, shown as the current plateau of the I-V curve as the voltage decreases. The modeled resulting photocurrent of the antenna is -60µA.

During flight the shield was maintained at a potential difference with the antenna, with an induced current from the spacecraft. Figure 5 shows the I-V curve of the shield, current of the shield with respect to the spacecraft versus the potential of the shield with respect to the antenna. This data could help the engineers and scientists select the necessary current needed to bias the voltage of the shield to reduce spurious currents from the shield to the antenna.

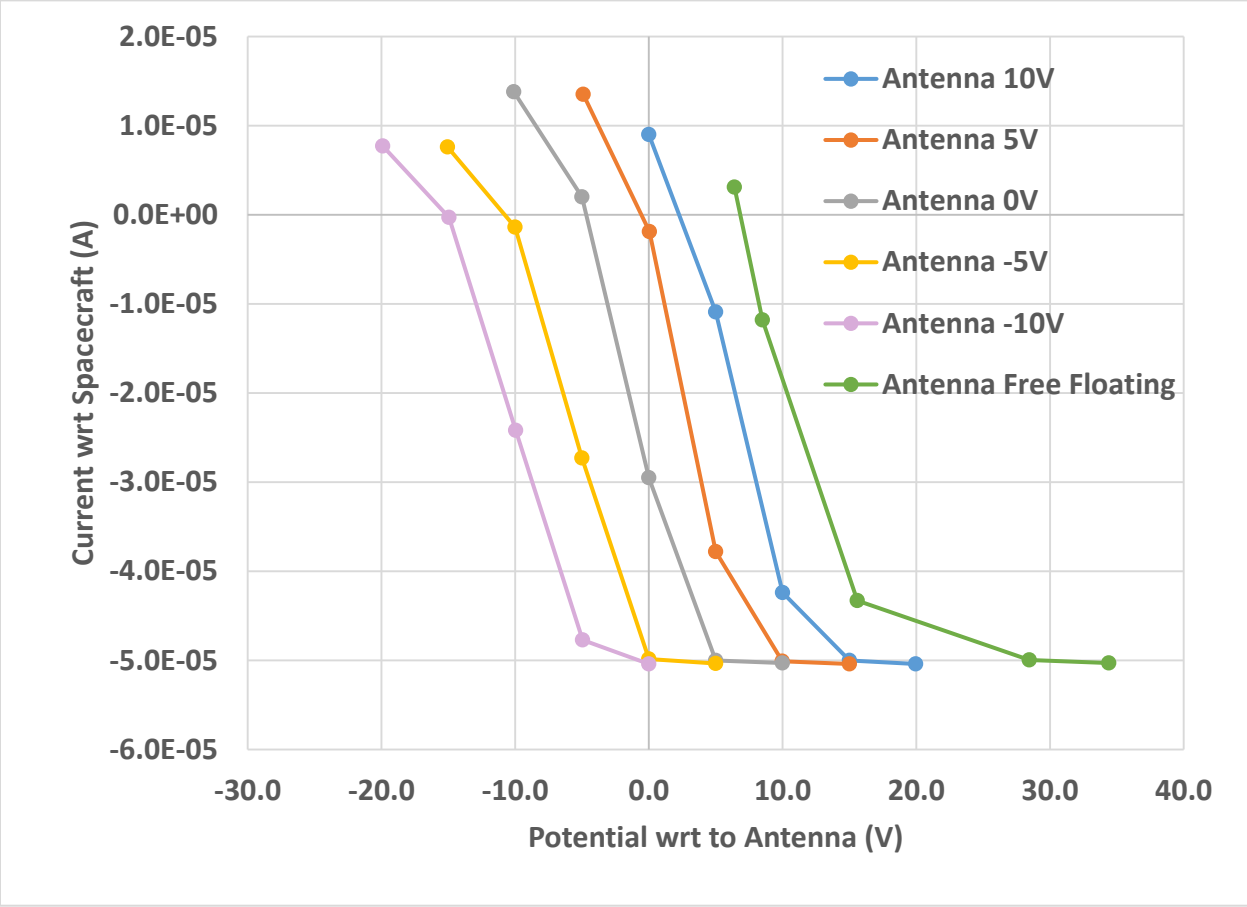

Figure 5 – Shield I-V Curve, Shield Current with respect to spacecraft vs. Potential with respect to Antenna

Figure 6 shows a special I-V curve of the shield, specifically the current of the shield with respect to the antenna versus the potential of the shield with respect to the antenna. Even though the shield and antenna are electrically isolated from each other in the model, there is an interaction of their plasma sheaths due to their proximity. This interaction behaves like a plasma channel and therefore a current can flow between them. To reduce this current, a shield potential

can be chosen depending on the antenna potential, i.e., if the antenna is at -5V bias, a -1V shield potential with respect to the antenna would give us a small -2.4µA current (compared to -51 µA with free floating shield). Such voltage biasing allows for more accurate measurements by reducing the current between the shield and the whip. It can be deduced from Figure 20 that this "base conductance" has an impedance of ~220 kΩ.

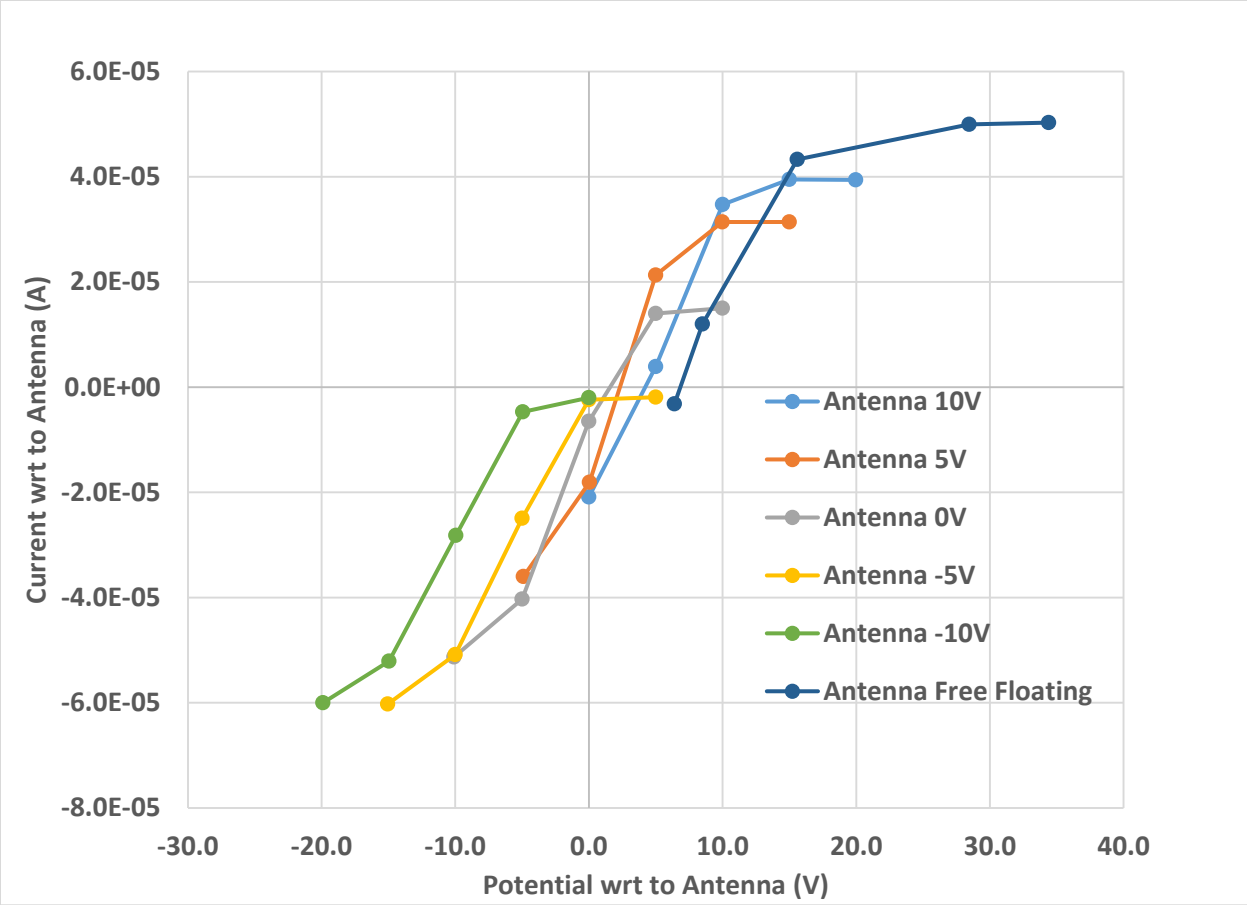

Figure 6 – Shield I-V Curve, Shield Current with respect to Antenna vs. Shield Potential with respect to Antenna

4.2 Flight Results

As mentioned in the last section, during the mission it was observed that the photocurrent yield of the Nb-C103 was 240 µA/m^2 at 1AU, more than double the value of the highest predicted from ground testing 118 µA /m^2 (unannealed) at an average of the max/min solar cycle. At the time of the flight measurement, the Sun was near the solar minimum (3rd quarter 2019), near the end of cycle 24.

The flight ambient plasma parameters at 35Rs are shown in Table 2. These parameters and the observed photocurrent values were introduced in the SPIS model, results shown in Table 4. Flight results suggest that the potential of the antenna charge more negative than the predicted potentials. In addition, if this larger Nb-C103 flight photoemission current compared to tested data remains unchanged during annealing of the Nb-C103, it will reduce the influence of the thermionic emission current in the current balance during closest approach at 9.8Rs.

Table 4– Model Potentials with 1st Perihelion, Flight Potential Bias Values (Antenna -11.6V and shield 0.1V), Flight Nb-C103 Photocurrent 2.4e-4A/m^2

	1st Perihelion (flight photocurrent no bias)	*1st Peihelion (flight photocurrent, bias)*	*Final Per. 9.5Rs (flight photocurrent, no bias)*
spacecraft	7.03	7.20	-12.9
Radiator	7.03	7.20	-12.9
TPS Foam	7.03	7.20	-12.9
TPS Shield	7.17	7.35	-12.9
FIELDS Shield	16.1	-4.33	2.95
FIELDS Antenna	22.5	-4.39	19.5

Figure 7 shows the plasma potential with the tested material properties and predicted environmental plasma parameters at 35Rs on the left, and the flight photocurrent properties and measured plasma potential on the right. Due to the larger photoelectron yield on the FIELDS antenna, the plasma potential changed near the instrument compared to the rest of the spacecraft.

During these first perihelia, the FIELDS antennas were held at -11.6V potential bias (-11µA)with respect to the spacecraft and with the shield at 0.1V potential bias with respect to the antenna. The antenna and shield potential predictions are not the same as the flight data, probably due to insufficient meshing and different plasma environment characteristics. However, there is sufficient qualitative and semi-quantitative agreement between the model and inflight results to allow for comparison use of one to interpret the other.

Figure 8 shows the voltage and current time series of the FIELDS PSP V1 through V4 antennas during the third encounter, on September 1, 2019. On the left axis the voltage measured is shown, while on the right axis the current sweep values are shown. There were four coplanar antennas measured, the results of the off plane fifth antenna are not shown.

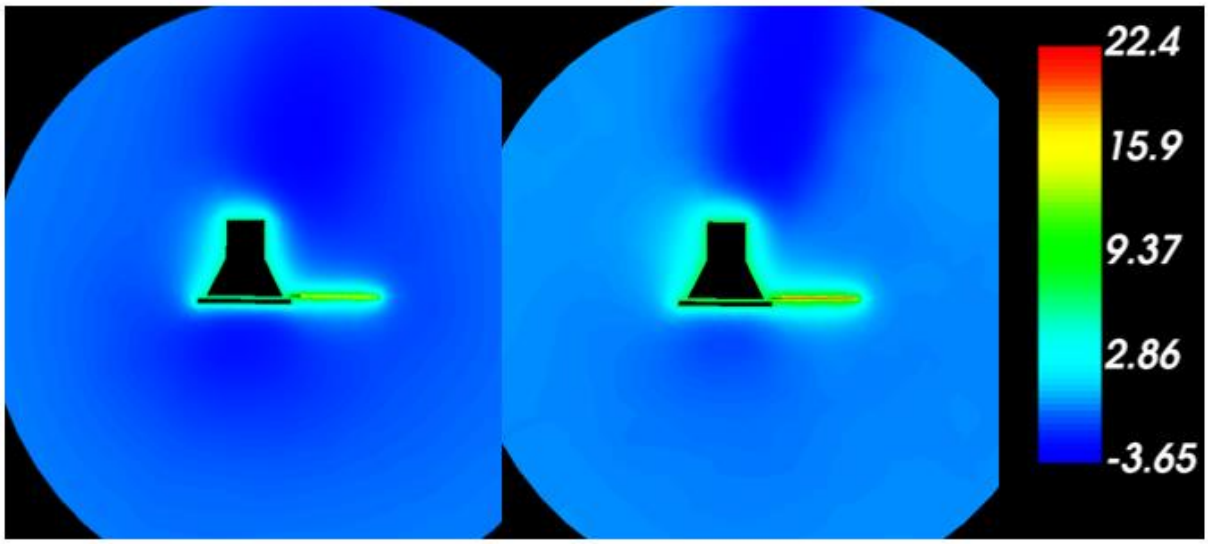

Figure 7 – Plasma Potential (Volts) of PSP at 35Rs a. Predicted Plasma Parameters and Tested Material Properties b. In-Situ Measured Plasma Parameters and Flight Photoyield

During the third perihelion there were four sweeps, two on V1 and V2 and two on V3 and V4. The first sweep performed on V1 and V2 was done with a current sweep between -100µA and 0 µA. The voltage of all four whips relative to spacecraft ground was measured at each step in the sweep. Like the first sweep, the second sweep was performed on V3 and V4 between -100µA and 0 µA. The third sweep was a smaller sweep, between -14 µA and 3.5 µA on V1 and V2. Finally, the fourth sweep was performed similarly between -14 µA and 3.5 µA on V3 and V4. Figure 23 also shows how the potentials of the fixed bias antennas during the current sweep change by a few volts, which could indicate a change in the spacecraft potential, influenced by the additional current required to support the biasing of the sweeping antennas. The inflight potential with respect to the spacecraft of the probes ranged between 2.9V and -1.9V compared to SPIS of 15.3V.

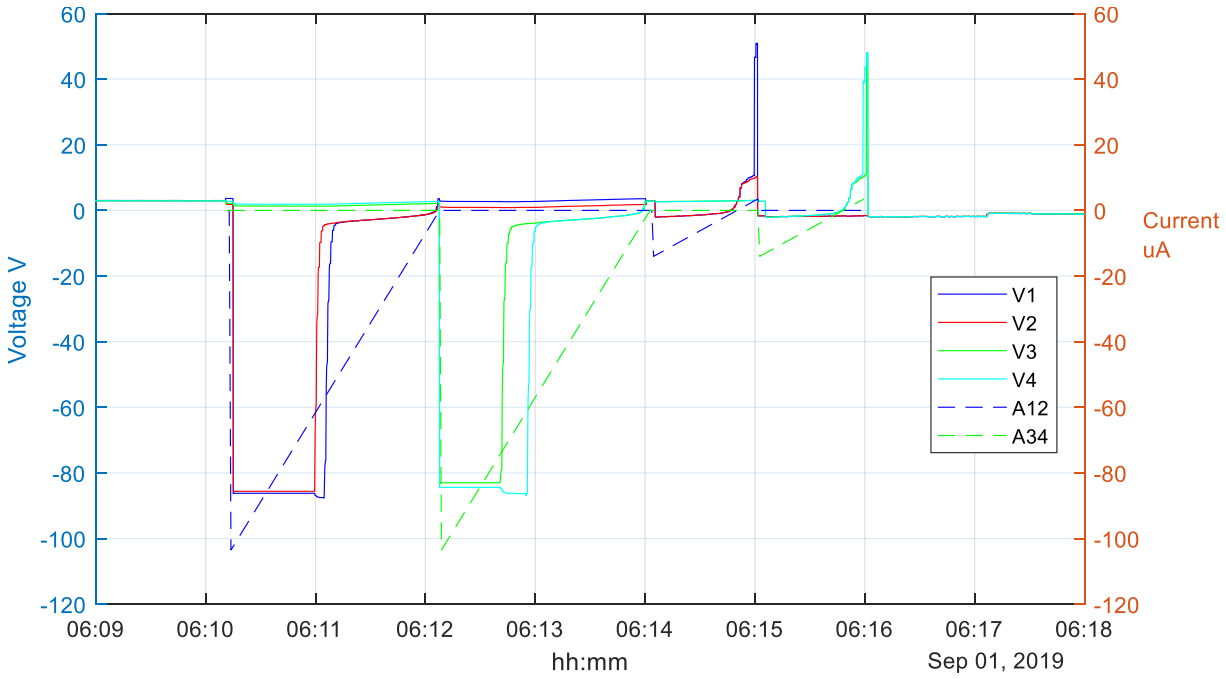

Figure 8 PSP FIELDS V1-V4 Antenna Voltage and Current Time Series

Figure 9 shows the PSP FIELDS antenna I-V curves for the first two sweeps. Figure 9 shows the antenna I-V curves for the second two sweeps. By comparing Figure 9 with Figure 4 from SPIS analysis, there are similarities worth mentioning, as the saturated current of the flight antennas are -52 µA, compared to the flight, between -54 µA and -72 µA. The space potential at the probe with respect to infinity is -4.3V for the data and -5V for the analysis.

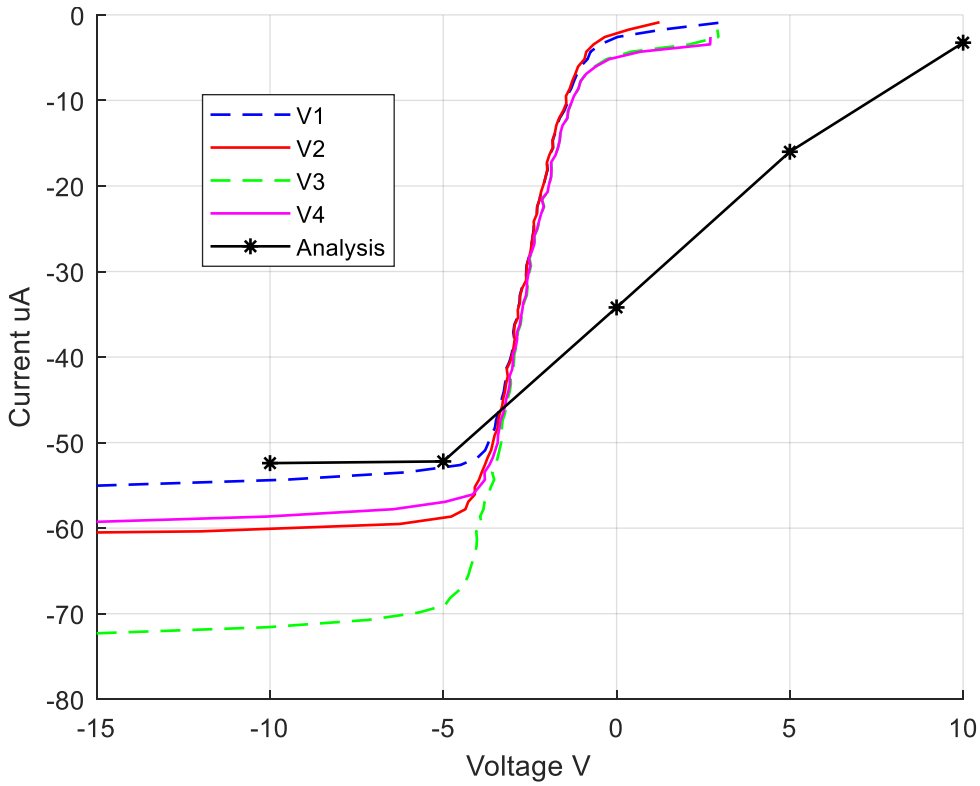

Figure 9– FIELDS V1-V4 Third Perihelion, First I-V Curve Sweep

The slopes of the I-V curve (or sheath impedances, as explained in 2.6, eq. 21) do differ, data giving an impedance of 51 kΩ, while the analysis gives a sheath impedance of 307 kΩ. These differences could be caused by the environmental differences between the analysis and the actual plasma environments, shown in Table 2, and geometrical differences between the shield and the antenna modeled versus flight.

Figure 10 shows another I-V curve forming at significant positive bias currents. As the bias current increases the antenna potential with respect to the spacecraft increases and then runs off towards the positive rail, probably due to saturation of the ambient electron current. This second I-V curve could be the signature of the I-V curve of the spacecraft sheath as described by [*Olson et al. '10*] for a Langmuir probe inside the spacecraft sheath, with an impedance value of 1 Mohm.

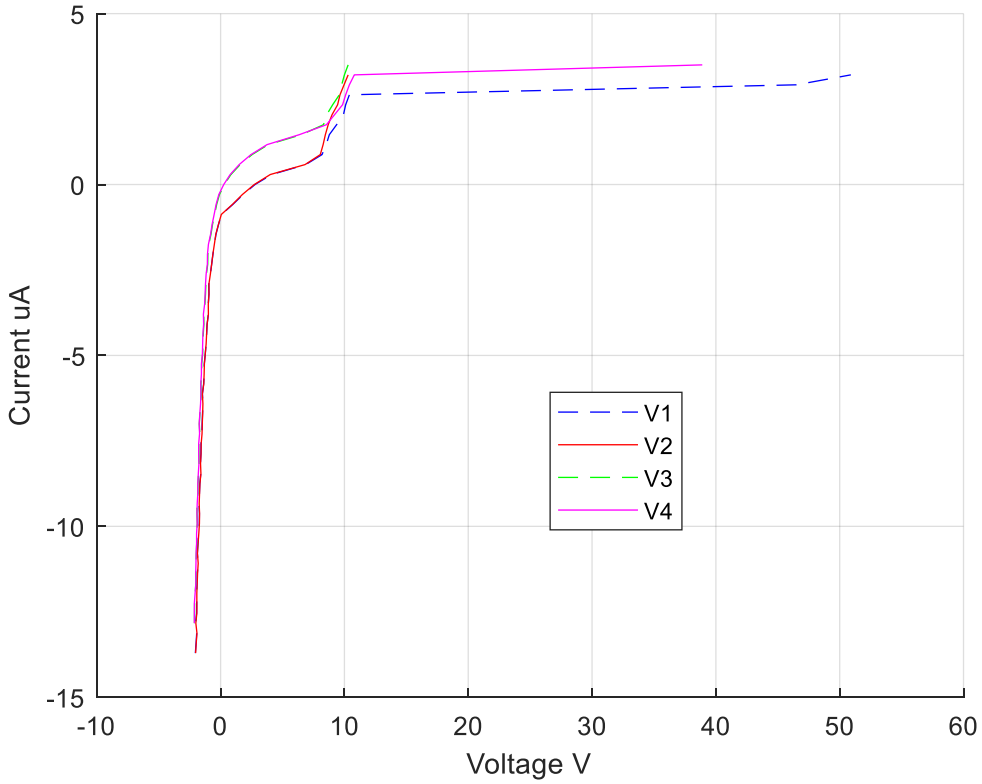

Figure 10 – FIELDS V1-V4 Third Perihelion, Second I-V Curve Sweep

5 Conclusions

The FIELDS antenna and shield I-V curves were shown for different shield potentials. An antenna bias current between -52μA and -22 μA is suggested for optimal measurement sensitivity. SPIS was also able to model the I-V curve between two electrically isolated surfaces, which were nevertheless coupled with each other through their sheath interactions with an impedance of 220kΩ. Based on those results, a negative voltage bias of the shield with respect to the antenna is recommended to reduce the spurious currents from the shield to the antenna.

Model results were then compared with initial flight results. The saturation photoelectron current of Nb-C103 was found to be greater than laboratory values by a factor of 2. The SPIS model was run with these new properties and the results were compared with flight values. Flight I-V curves were plotted and compared to the analysis. Current saturations were found to be within the same order of magnitude and similar potentials with respect to infinity were observed. The slopes of the I-V curve (and therefore the sheath impedances) differed greatly,

51kΩ in flight versus 307kΩ. Even though it was found that FIELDS antenna potentials were more negative than predicted when not current biased, there could be certain advantages for spacecraft charging engineers, and therefore scientists in obtaining the I-V curves during the design process using SPIS.

Acknowledgments, Samples, and Data

Millan D.A. would like to thank David Glaser, Chris Scholtz, Marc Pulupa at Space Sciences Laboratory. He would also like to thank Julien Forest, Benjamin Ruard, Arnaud Trouche, and Jean-Charles Mateo Velez for their SPIS modeling feedback. This work was partially supported by the NASA PSP FIELDS contract NNN06AA01C. Flight and environmental data used in this paper are publicly available at http://fields.ssl.berkeley.edu/data. Model data are available at Zenodo, TBD link.

References

1 Andersson, L., et al. (2015). "The Langmuir Probe and Waves (LPW) Instrument for MAVEN." Space Science Reviews **195**(1): 173-198.
2 Bale, S. D., et al. (2019). "Highly structured slow solar wind emerging from an equatorial coronal hole." Nature **576**(7786): 237-242.
3 Bale, S. D., et al. (2016). "The FIELDS Instrument Suite for Solar Probe Plus." Space Science Reviews **204**(1-4): 49.
4 Bonnell, J. W., et al. (2008). "The Electric Field Instrument (EFI) for THEMIS." Space Science Reviews **141**(1): 303-341.
5 Cully, C. M., et al. (2007). "Electrostatic structure around spacecraft in tenuous plasmas." Journal of Geophysical Research: Space Physics **112**(A9): n/a-n/a.
6 Diaz-Aguado, M., et al. (2019). "Experimental Investigation of Total Photoemission Yield from New Satellite Surface Materials." AIAA Journal of Spacecraft and Rockets **56**(1): 248-258.
7 Diaz-Aguado, M., et al. (2020). "Parker Solar Probe FIELDS Iinstrument Ccharging in the Nnear- Sun Eenvironment:
Part I – Computational Model." Journal of Geophysical Research: Space Physics **To be submitted**.
8 Diaz-Aguado, M. F., et al. (2020). "Experimental Investigation of the Secondary and Backscatter Electron Emission from New Spacecraft Surface Materials." AIAA Journal of Spacecraft and Rockets **TBD**(TBD).
9 Donegan, M. M., et al. (2014). Surface Charging Predictions for Solar Probe Plus. Spacecraft Charging Technology Conference. Pasadena. **134**.
10 Donegan, M. M., et al. (2010). "Spacecraft Coating-Induced Charging: Materials and Modeling Study of Environmental Extremes." Journal of Spacecraft and Rockets **47**(1): 134-146.
11 Ergun, R. E., et al. (2010). "Spacecraft charging and ion wake formation in the near-Sun environment." Physics of Plasmas **17**(7): 072903.
12 Feuerbacher, B., et al. (1972). "Experimental Investigation of Photoemission from Satellite Surface Materials." Journal of Applied Physics **43**(4): 1563-1572.
13 Garrett, H. B. (1981). "The charging of spacecraft surfaces." Reviews of Geophysics **19**(4): 577-616.
14 Grard, R. J. L. (1973). "Properties of the satellite photoelectron sheath derived from photoemission laboratory measurements." Journal of Geophysical Research **78**(16): 2885-2906.

15 Guillemant, S., et al. (2012). "Solar wind plasma interaction with solar probe plus spacecraft." Annales Geophysicae **30**(7): 1075.
16 Gurnett, D. A., et al. (2004). "The Cassini Radio and Plasma Wave Investigation." Space Science Reviews **114**(1): 395-463.
17 Gurnett, D. A., et al. (1995). "The Polar plasma wave instrument." Space Science Reviews **71**(1-4): 597-622.
18 Gustafsson, G., et al. (1997). "The Electric Field and Wave Experiment for the Cluster Mission." Space Science Reviews **79**(1): 137-156.
19 Hastings, D., et al. (1996). Spacecraft-Environment Interactions. New York, Cambridge University Press.
20 Kasper, J. C., et al. (2019). "Alfvénic velocity spikes and rotational flows in the near-Sun solar wind." Nature **576**(7786): 228-231.
21 Laakso, H., et al. (1995). "Plasma gradient effects on double-probe measurements in the magnetosphere." Annales Geophysicae **13**(2): 130-146.
22 Marchand, R., et al. (2014). "Cross-comparison of spacecraft-environment interaction model predictions applied to Solar Probe Plus near perihelion." Physics of Plasmas **21**(6).
23 McComas, D. J., et al. (2019). "Probing the energetic particle environment near the Sun." Nature **576**(7786): 223-227.
24 Mott-Smith, H. M., et al. (1926). "The theory of collectors in gaseous discharges." Physical Review **28**(4): 727-763.
25 Mozer, F. S., et al. (1979). "The dc and ac electric field, plasma density, plasma temperature, and field-aligned current experiments on the S3-3 satellite." Journal of Geophysical Research: Space Physics **84**(A10): 5875-5884.
26 Mullen, E. G., et al. (1986). "SCATHA survey of high-level spacecraft charging in sunlight." Journal of Geophysical Research: Space Physics **91**(A2): 1474-1490.
27 Olson, J., et al. (2010). "On the interpretation of Langmuir probe data inside a spacecraft sheath." Review of Scientific Instruments **81**(10).
28 Pedersen, A. (1995). "Solar wind and magnetosphere plasma diagnostics by spacecraft electrostatic potential measurements." Annales Geophysicae **13**(2): 118-129.
29 Pedersen, A., et al. (1984). "Quasistatic electric field measurements with spherical double probes on the GEOS and ISEE satellites." Space Science Reviews **37**(3): 269-312.
30 Roussel, J. F., et al. (2008). "SPIS Open-Source Code: Methods, Capabilities, Achievements, and Prospects." IEEE Transactions on Plasma Science **36**(5): 2360-2368.
31 Thiebault, B., Mateo Velez, J-C. Forest, J., Sarrailh, P. (2013). "SPIS 5.1 User Manual."
32 Torbert, R. B., et al. (2016). "The FIELDS Instrument Suite on MMS: Scientific Objectives, Measurements, and Data Products." Space Science Reviews **199**(1-4): 105.
33 Vaivads, A., et al. (2007). "Low-frequency electric field and density fluctuation measurements on Solar Orbiter." Advances in Space Research **39**(9): 1502-1509.
34 Whipple, E. C. (1981). "Potential of Surfaces in Space." Report on Progress of Physics **44**: 1197-1250.
35 Whipple, E. C., Jr. (1965). The equilibrium electric potential of a body in the upper atmosphere and in interplanetary space - NASA-TM-X-55368, Sponsoring Organization: NASA Goddard Space Flight Center.
36 Wygant, J. R., et al. (2013). "The Electric Field and Waves Instruments on the Radiation Belt Storm Probes Mission." Space Science Reviews **179**(1): 183-220.